Available online at www.sciencedirect.com
SCIENCE DIRECT®
International Journal of Heat and Mass Transfer 48 (2005) 2613–2624
International Journal of HEAT and MASS TRANSFER
www.elsevier.com/locate/ijhmt

Efficient defrosting of an inclined flat surface

Subrata Roy *, Haribalan Kumar, Richard Anderson

Computational Plasma Dynamics Laboratory, Kettering University, Flint, MI 48504, USA

Received 1 January 2005; received in revised form 31 January 2005
Available online 26 March 2005

Abstract

We present a deicing simulation for a practical three-dimensional geometry inside which hot air jets impinge upon a flat inclined glass surface with a layer of ice on the outside. The main goal is to study the unsteady two-phase melting process over the inclined flat surface, and to identify the traditional control parameters such as jet impingement angles for minimization of the defrosting time for given ice and glass thicknesses. A correlation for defrosting as functions of time, heat transfer parameters and impingement angles has been found. Also, in this study, the first Joule heating defroster using transparent electrodes are proposed and numerically simulated as a viable alternative. A correlation between the electrical Joule power requirement and the defrosting time is given. It is demonstrated that substantial improvements (roughly 70% reduction) in defrosting time may be achieved using Joule heating compared to the traditional jet impingement HVAC technology.

Keywords: Vehicle climate control; CFD; Conjugate heat transfer; Joule heating; Jet impingement; Deicing/defrosting

1. Introduction

The jet impingement heat transfer has many practical applications including windshield defrosting and defogging for automotive and aircraft applications. Specifically on a flat surface, several experimental and numerical studies of impinging air jets have been reported over the past three decades [1–10]. Most of these computational efforts are focused on modeling the heat transfer without the phase change. Recently, several researchers have focused on the deicing patterns over the windshield [11–13] and aircraft wings [14]. These reports range from a patent on fluidic oscillators for better flow and heat transfer patterns [11] to the theoretical prediction and computation of ice formation [14]. Automotive engineers have applied commercial software such as fluent, ICEM-CFD and Star-CD to predict the melting of ice over the windshield and compared results with thermography and hot bulb type of measurements [12]. However, a correlation for defrosting as functions of time, flow and heat transfer parameters and impingement angle is yet to be found.

Deicing is a two-phase fluid thermal process for removal of a thin ice layer on the exterior surface of a vehicle windshield and is required to be done in the quickest possible manner for driver visibility in the wintry conditions. A traditional defroster uses a simple electric fan to push air that has been heated by the engine coolant lines into a gap between the top of the blower ductwork and the top panels of dashboard trim. Into the trim panel several slots have been cut, separated by directional vanes. These vanes control the left–right

* Corresponding author. Tel.: +1 810 762 9949; fax: +1 810 762 7985.
E-mail address: sroy@kettering.edu (S. Roy).

0017-9310/$ - see front matter © 2005 Elsevier Ltd. All rights reserved.
doi:10.1016/j.ijheatmasstransfer.2005.01.022

Nomenclature

C	coefficients
c_p	specific heat at constant pressure kJ/kg K
E	specific enthalpy, kJ/kg
F	light transmittance
H	convection heat transfer coefficient, W/m^2 K
k	thermal conductivity, W/m K
L	characteristic length, m
Nu	Nusselt number
P	power spent in Joule heating, kW
$\dot{Q}$	heat transfer rate, W
Re	Reynolds number
S_J	source term (Joule heat)
S_L	source term (latent heat)
t	time, s
T	temperature, K
u_i	ith component of velocity, m/s
V	jet velocity, m/s
x_i	spatial coordinates, m

Greek symbols

λ	liquid fraction
Λ	latent heat, kJ
μ	viscosity, N s/m^2
ρ	density, kg/m^3
σ	bulk resistivity, Ω m
ϖ	applied potential, V

Subscripts

A	Case A
avg	average
B	Case B
eff	effective
in	inlet (at nozzle exit)
i, j	direction of spatial derivatives
L	liquidus
M	mush
ref	reference
s	slip between ice and water
S	solidus
w	wall

angle between the plane of the windshield and the incoming warm air. The fore-aft placement of the blower vents in the top of the dashboard (and any beveling of the vent edges) controls the angle of incidence between the warm air and the windshield. This arrangement relies on both convection and conduction to transfer the heat to the outside of the windshield and the layer of ice atop it. Recently, Roy and Patel [6] have investigated the effect of Reynolds number (Re) and impingement angles on local and average Nusselt number (Nu), turbulence intensity and wall y^+. They have determined a correlation between the geometric angles and the fluid thermal characteristics on the inner surface of the windshield. Here the particular interest is to study defrosting on the outer surface of the glass windshield for improved vehicle climate control enhancing passenger safety and comfort. Two different defrosting methods have been considered. First, a traditional windshield arrangement with jet impingement is analyzed. The intention is to predict a two-phase correlation that will guide future design of windshield defroster. Hereafter we call this Case A. Next, an alternative electrothermal defrosting mechanism is proposed and analyzed. Hereafter this is referred to as Case B. As far as we know, this is the first time such analyses are reported.

Fig. 1 shows the jet, the inclined plane and its association with the control volume bounded by five other surfaces for Case A. All necessary dimensions are given in the figure. The temperature T_j of the air jets vary based on the blower data plotted in Fig. 2. The jets ensue from two rectangular openings (each 0.019 m × 0.241 m) and impinge upon the target solid surface of thickness 0.006 m and known material properties with various streamwise (ϕ) and crosswise (β) angles. A thin sheet of 0.0004 m thickness initially filled with ice is attached to the outer layer of the target plane. The rectangular openings are centered on the 1.447 m length of the bottom wall with an edge-to-edge gap of 0.127 m between them. The target plane is inclined at an angle of 39°. We investigate the melting patterns of ice at four different time stations. An optimum jet impingement angle is found for the most effective melting of ice that conforms to the defrosting standard [15] for the automotive community.

A Joule heating defroster using transparent electrode is numerically simulated in case B as a viable alternative. In this arrangement, a current runs through a highly resistive electrode, preferably one with a high conductive heat transfer coefficient k, and dissipates heat proportional to the dot product of the electric field and current. Fig. 3 shows the schematic arrangement of glass and electrode for Case B. Here 0.0001 m thick indium tin–oxide (ITO), with high thermal and low electrical conductivity is used between the two 0.003 m glass layers. It is optically transparent (95% transmittance), thus does not interfere with the vision of the driver. The ITO resists the current dissipating energy as Joule heating. This heat is conducted through the glass to the ice layer outside and eventually melts it. The ITO layer is the same dimension

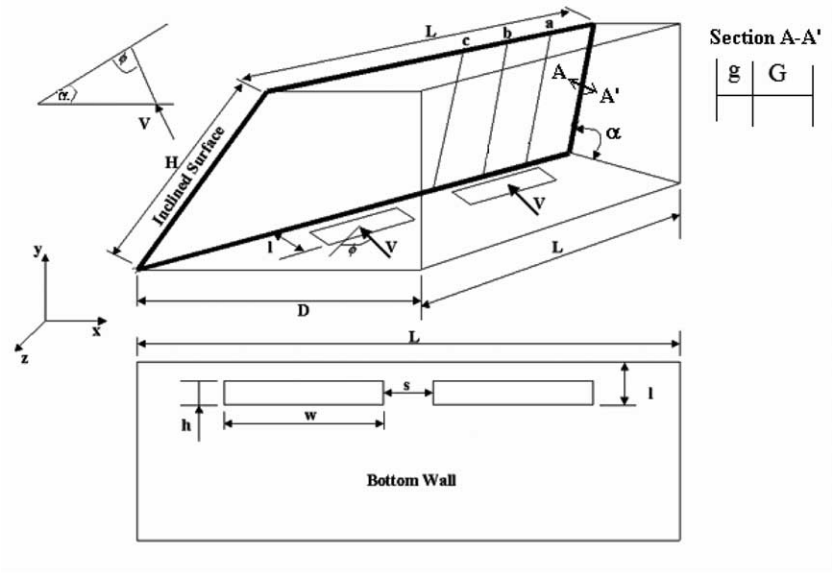

Length of Inclined surface, L	1.447 m
Width of inclined surface, H	0.719 m
Surface inclination angle, α	39°
Shield surface thickness, G	0.006 m
Ice layer thickness, g	0.0004 m
Location of nozzle, l	0.134 m
Length of nozzle exit plane, h	0.019 m
Width of nozzle exit plane, w	0.241 m
Jet impingement angle, ϕ (on x-y plane)	21° – 66°
Sweep angle, β (on y-z plane)	5°, 10°
Span of bottom wall, D	0.896 m
Distance between nozzle exit planes, s	0.127 m

Fig. 1. Schematic of computational domain of the windshield and the associated air volume.

as the windshield. The predicted performance results are compared against the current jet impingement HVAC technology with respect to requirements in both time and power to melt the ice. It is demonstrated that substantial improvements in defrosting time (roughly 70% reduction in clearing time) may be made implementing the suggested design, which uses joule heating.

Three correlations are established—one between jet impingement angles and melting characteristics of ice (case A), the average Nusselt number evolution during defrosting (case A), and finally predicted electrical power requirement in the proposed Joule heating defroster as a function of time (case B).

2. Theoretical formulation

The fluid–thermal processes in the computational domain are investigated using a finite volume based commercial code Fluent6.1.22©. The details of the flow code are given earlier [5,6]. Here the deicing simulation is performed in two stages. First the steady state flow characteristics of air are analyzed for the impinged jets with renormalized group (RNG) two-equation k–ε turbulence closure model [16] by solving the continuity and momentum equations as given in Ref. [6]. Then the unsteady conjugate heat transfer calculations are done between air, windshield material and ice for the

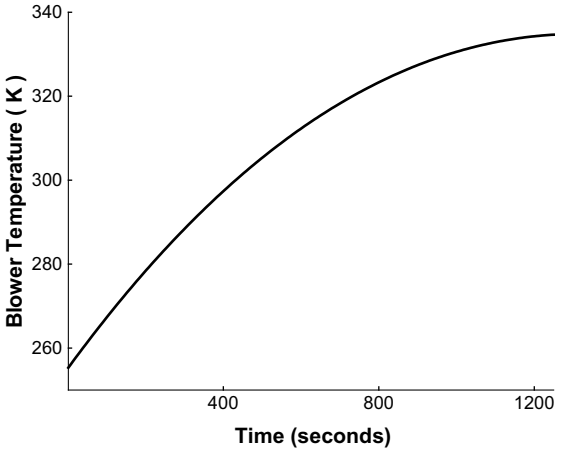

Fig. 2. Blower temperature curve plotted as a function of time.

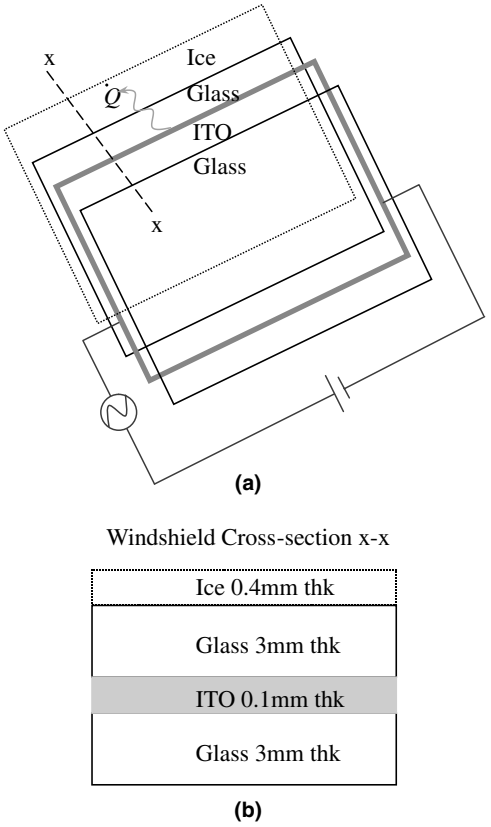

Fig. 3. Schematic of a windshield with Joule heating defroster.

time varying jet temperature while maintaining the air velocity profiles steady. The energy equation solved for this step is given as

$$\frac{\partial(\rho E)}{\partial t}+\frac{\partial(\rho u_i E)}{\partial x_i}=\frac{\partial}{\partial x_i}\left(k\frac{\partial T}{\partial x_i}\right)+S_{\mathrm{J}}+S_{\mathrm{L}} \tag{1}$$

where E is enthalpy, ρ is the density, u_i is the ith component air velocity, k is the conductivity, S_{J} is the energy density supplied through Joule heating and S_{L} is the source term defined based on the Carman–Koseny equation [17]

$$S_{\mathrm{L}}=C_{\mathrm{m}}\frac{(1-\lambda)^2}{\lambda^3+\varepsilon}\,(u_{\mathrm{m},i}-u_{\mathrm{s},i}) \tag{2}$$

In (2), λ is the liquid fraction, ε is a small number ($\sim 10^{-3}$) used to prevent division by zero, C_{m} is the mushy zone constant ($\sim 10^5$), which measures the amplitude of damping. Higher values of these coefficients result in steeper transition of velocity between solid and liquid regions. The porous velocity components of the mush $u_{\mathrm{m},i}$ is calculated from the Darcy law. We have considered negligible slip velocity between solid and melting zones $u_{\mathrm{s},i}$ and thus ignored the relative velocity between the solid ice and melted mush.

The following two-phase solidification and melting enthalpy-porosity formulation is used to model the melting of ice on the outer surface [18].

$$E=\left(E_{\mathrm{ref}}+\int_{T_{\mathrm{ref}}}^{T}c_p\mathrm{d}T\right)+\Delta E \tag{3}$$

The first term in the right hand side of (3) (the terms inside the parentheses) is the sensible heat where the reference enthalpy E_{ref} = 298 kJ/kg, and $\Delta E=\lambda\Lambda$ is the latent heat content which varies from zero to Λ determined by the liquid fraction λ given below,

$$\lambda=\frac{T-T_{\mathrm{s}}}{T_{\mathrm{L}}-T_{\mathrm{s}}},\quad 0\leqslant\lambda\leqslant 1. \tag{4}$$

The static temperature of ice, windshield and its associated air volume is calculated by iterating Eqs. (1)–(3) with liquid fraction λ being updated at each step. Table 1 lists all the material properties and reference temperatures used for solving the two-phase conjugate heat transfer for both cases.

3. Numerical details

3.1. Case A

The mean velocity of the jet V is chosen to be 8 m/s for which the Reynolds number for air is 20000 based on the hydraulic diameter of the rectangular opening. As tabulated in Table 2, the impingement angle ϕ is varied from 21° to 66° in steps of 15° in the xy-plane and then the sweep angle β is varied from 0° to 10° in steps of 5° in the outward direction in the yz-plane. The jet openings are in plane with the bottom floor for all these experiments making the floor jet injection angle $(180^\circ-\phi-\beta)$ varying between 75° and 120°. The intersection of the jet axis and the inclined surface is $(0.09674+0.07831/\tan\phi)$ m away from the crotch. The

Table 1
Material properties

Material	Properties
Glass	$\rho = 2500$ kg/m^3, $c_p = 0.750$ kJ/kg K, $k = 1.4$ W/m K
Ice	$\rho = 920$ kg/m^3, $c_p = 2.040$ kJ/kg K, $k = 1.88$ W/m K, $\Lambda = 334.96$ kJ/kg, $T_S = 271$ K, $T_L = 273$ K, $\mu = 0.00553$ N s/m^2
ITO	$\rho = 7140$ kg/m^3, $k = 8.7$ W/m K, $F = 95\%$, $\sigma = 2 \times 10^{-6}$ Ω m
Air	$\rho = 1.225$ kg/m^3, $c_p = 1.00643$ kJ/kg K, $k = 0.0242$ W/m K, $\mu = 1.789$ e−05 N s/m^2

outlet at the back has a hydraulic diameter of 0.625 m where the backflow turbulence intensity is given as 10% while a backflow temperature of 273 K is assumed. Hereafter we will refer to inner surface of the windshield as IN; interface between the layers of ice and the glass as MID and the outer wall of the ice layer as OUT for clarity. Fluent treats MID and IN as coupled surfaces as they are two-sided walls appearing between the ice and glass, and glass and air, respectively. The heat transfer is calculated directly from the solution in adjacent cell. It is assumed OUT is close to temperature of ice and the ambient air velocity "outside" the simulation domain is negligible. All other walls are considered adiabatic. We solved the fluid and heat transfer equations on a computational mesh of 216 319 nodes created using T-Grid. The windshield and ice layer consist of hexagonal elements/laminates with 18 432 nodes in the windshield and 6912 in the ice layer. The Newton iteration is considered converged when the solution residual for all variables except temperature is less than 10^{-4} and for energy it is less than 10^{-7}.

3.2. Case B

Here the jet impingement is not considered. Only the glass and the ice layer are simulated. Here again, we assume OUT is at the temperature of ice and the ambient air velocity is negligible. All other walls are considered adiabatic except for IN surface where $H = 5$ W/m^2 K is applied. There is no air flowing in this system. We solved only the energy equations on a computational mesh created using T-Grid meshing scheme (for details, refer Gambit manual). Each glass layer in Fig. 3b consists of 69 741 nodes, the ITO has 16 605 nodes and the ice layer contains 29 889 nodes for computation. The Newton iteration is considered converged when the solution residual for energy is less than 10^{-7}. The electrical circuit is not in the scope of this paper. However, note that the power dissipated per unit area of the ITO is proportional to ϖ^2/σ which gives the applied energy density S_J to the ITO. The glass is assumed as perfect electrical insulator.

For both cases, the windshield is considered as "cleared" or "defrosted" when the MID surface conforms to the standards of SAE J902. Fig. 4 shows the two important regions A and C on the windshield for which the acceptable defrosted minima are recommended in the automotive standard [15]. In figure, the normal distance from P to eye is 0.6 m, the eye E is 0.3 m away from the side of the vehicle and the height H from the driver seat to E is 0.635 m. The automotive requirement for defrosting in Table 3, where the details of regions A and C are also given, shows that while all of region C needs to be cleared region A may not require the total removal of ice.

4. Results and discussion

4.1. Case A

Figs. 5–13 describe twelve simulation results for case A. The best and worst performances of deicing are highlighted in bold and in italics, respectively, in Table 2.

Table 2
Twelve simulation cases tested for various jet angles

α (deg)	ϕ (deg)	$180 - (\alpha + \phi)$ (deg)	β (deg)	% of A that melted in 1200 s	% of C that melted in 1200 s
39	66	75	0	87	82
			5	91	99
			10	90	93
	51	90	0	84	75
			5	93.5	100
			10	**99**	**100**
	36	105	0	77	64
			5	88.4	85.7
			10	95	100
	21	120	*0*	*62*	*28.5*
			5	71	50
			10	68	57

The best and worst performances of deicing are highlighted in bold and in italics, respectively.

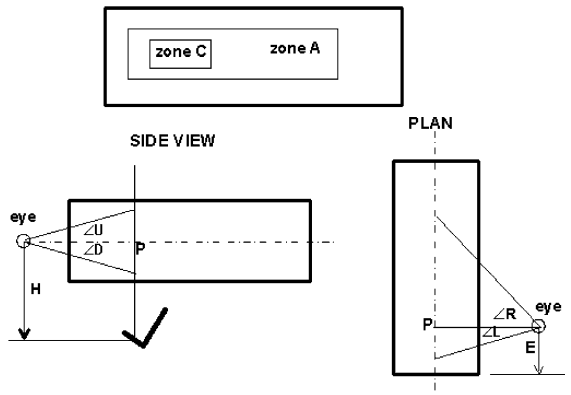

Fig. 4. SAEJ902 standard for windshield vision [15].

Table 3
SAEJ902 standard for defrosting in 30 min with steady air jet

Zone	Minimum %	Angle L (deg)	Angle R (deg)	Angle U (deg)	Angle D (deg)
A	80	18	56	10	5
C	100	10	15	5	1

For jet angles $\phi = 51°$ and $\beta = 10°$, all ice melts in regions A (99%) and C (100%) within 20 min. Hereafter, this is referred to as the best arrangement. The worst occurs for $\phi = 21°$ and $\beta = 0°$ where only 29% of C and 62% of A defrosts within 20 min. Hereafter, we refer to this case as the worst arrangement. Fig. 5 plots the liquid fraction λ distribution on the MID windshield surface at four different time stations, namely 400 s, 600 s, 900 s and 1200 s. At 400 s only 2.3% of the ice is melted at two impingement regions, by the time it reaches 600 s 85.7% of the ice about the impingement regions is melted. Interestingly, the jets issued from rectangular slots with high aspect ratios create near circular footprints on the windshield. Ice melts completely in the C region and nearly 98.8% for the region A within the mandated 20 min.

In comparison, Fig. 6 shows line contours of λ on the MID surface at 600 s, 700 s, 900 s and 1200 s for the worst arrangement. While for the best arrangement it takes about 400 s for the ice to start melting, no significant melting starts before 600 s for the worst arrangement. After 20 min only the central region melts, keeping half of regions A and C frozen. The details of melting after 20 min along three specific lines a, b and c (Fig. 1) on the MID surface are shown in Fig. 7 for two impingement angles ($\phi = 21°$ and 36°) and three sweep angles ($\beta = 0°$, 5° and 10°). The computed solid fraction (1-λ) data along these lines are projected on the x direction for plotting purposes. The location $x = 0$ is the intersection between the windshield and the bottom wall. The impingement angle ϕ has significant impact along the selected lines a, b and c. For $\phi = 36°$, the melting increases significantly as compared to $\phi = 21°$. The performance is even better for $\phi = 51°$ (not shown). Note that line b is exactly on the impinge-

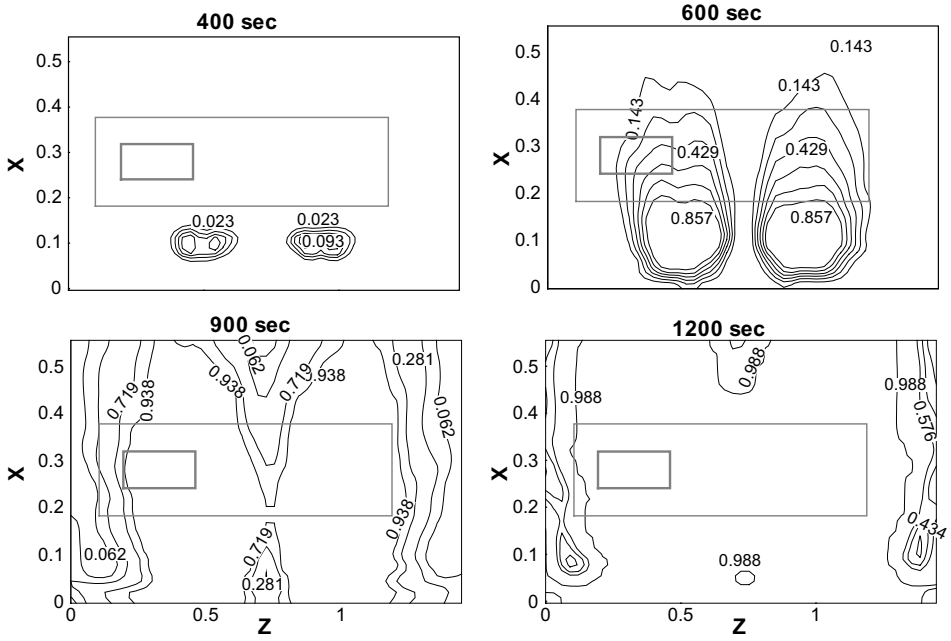

Fig. 5. Time evolution of the liquid fraction distribution for the best arrangement.

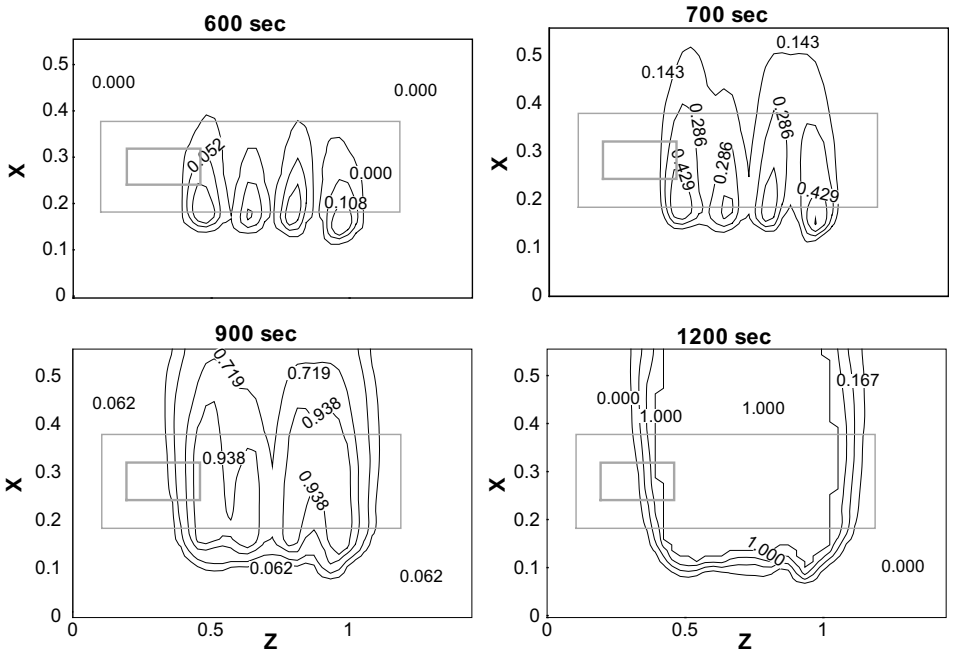

Fig. 6. Time evolution of the liquid fraction distribution for the worst arrangement.

ment zone and there is not much effect of β on the melting characteristics along this line. For line a, which is closest to the driver's vision, the melting characteristic improves as β increases. However, there is an inverse relation between β and the melting characteristic for line c, which is the furthest from the driver's eye. This is obvious as line c lies between impingement zones. The flow details for these solutions are given in our previous work [5,6] showing the regions of minor flow and major flow separated about the point of impingement.

Fig. 8 summarizes the area average liquid fraction, $\lambda_{avg} = (\int_A \lambda dA)/A$, for 12 test cases given in Table 2. Fig. 8a plots a quadratic polynomial fit for the data calculated based on the windshield area A. Note that we avoided the power fit representation of the data as that will fail to indicate the optimum operating range of ϕ between 50° and 60°. While $\beta = 10°$ shows the best performance, the following three correlations are established for $0° \leqslant \beta \leqslant 10°$ and $0° \leqslant \phi \leqslant 75°$.

(1) For $\beta = 0°$, $\lambda_{avg} = -0.48\phi^2 + 1.22\phi + 0.02$
(2) For $\beta = 5°$, $\lambda_{avg} = -0.95\phi^2 + 1.97\phi - 0.15$
(3) For $\beta = 10°$, $\lambda_{avg} = -1.4\phi^2 + 2.64\phi - 0.31$

The λ_{avg} calculated based on the mandated regions of C and A of the windshield is given in Fig. 8b and c, respectively. For both regions $\beta = 0°$ gives the worst performance. In the region C in Fig. 8b, the predicted λ_{avg} for the jet sweep $\beta = 5°$ and 10° follow each other closely beyond $\phi > 25°$. The trend is similar in Fig. 8c for region A also.

Understanding the heat transfer characteristics is vital to understand the melting process. Figs. 9 and 10 demonstrate the enthalpy contour evolution on the MID surface of the windshield for the best and worst arrangements. The enthalpy increases sharply between 300 and 600 s from 12 kJ/kg to 323 kJ/kg and then reaches finally to a peak of 415 kJ/kg at 1200 s in Fig. 9. The predicted enthalpy distribution for the worst arrangement in Fig. 10 also shows the gradual increase in enthalpy from 10 kJ/kg to 395 kJ/kg. However, the average enthalpy of the best arrangement is nearly twice than that of the worst. Figs. 11–13 plot the Nusselt number distribution on the IN surface of the windshield. IN is exposed to impinging jets. Fig. 11 shows the time evolution for best arrangement with a Nu ranging from 4 to 12. Clearly, maximum heat transfer happens about jet impingement points. For the worst arrangement, the Nu distribution shows fingerlike patterns near the impingement region in Fig. 12 similar to the liquid fraction (Fig. 6) and enthalpy (Fig. 9) distributions. The peak Nu after 20 min is only a quarter of that of Fig. 11. It is the fluid–thermal interaction described in Ref. [6] that may cause these patches and, in effect, poor heat transfer. For these acute impingement angles of $\phi = 21°$ and $\beta = 0°$, the jet attaches to the upper lip of the windshield and does not get enough contact with glass to inject heat carried by the blower air.

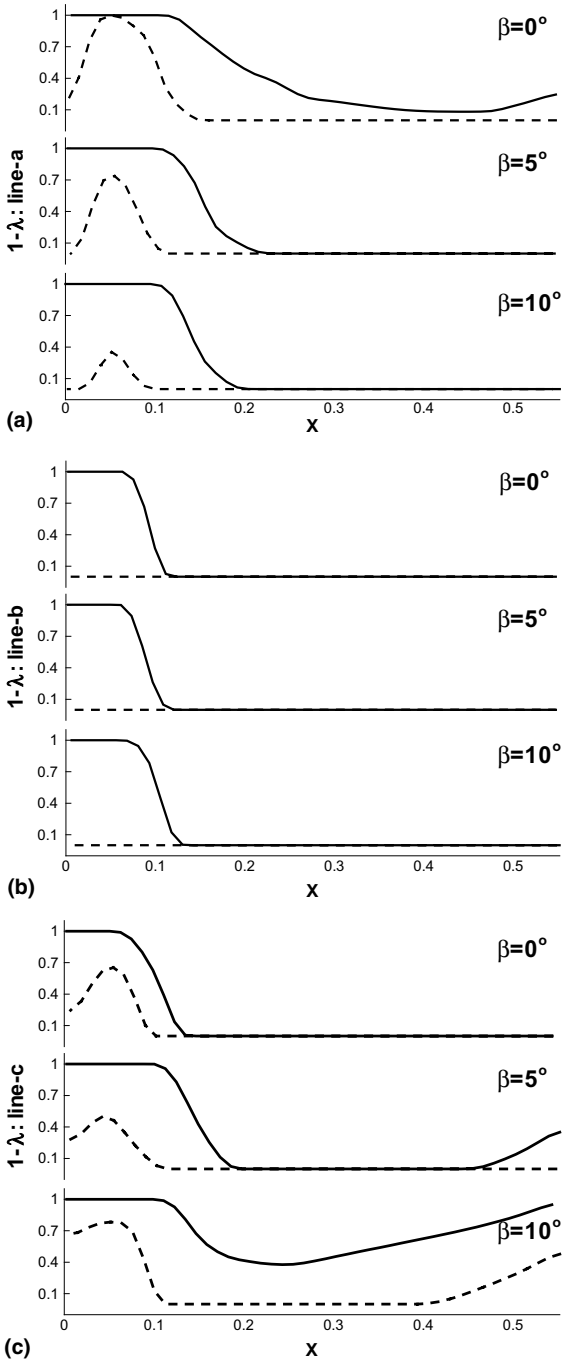

Fig. 7. Solid fraction distribution on selected lines a, b, c at time = 1200 s (see Fig. 1). Solid line represents $\phi = 21°$ and dotted line represents $\phi = 36°$.

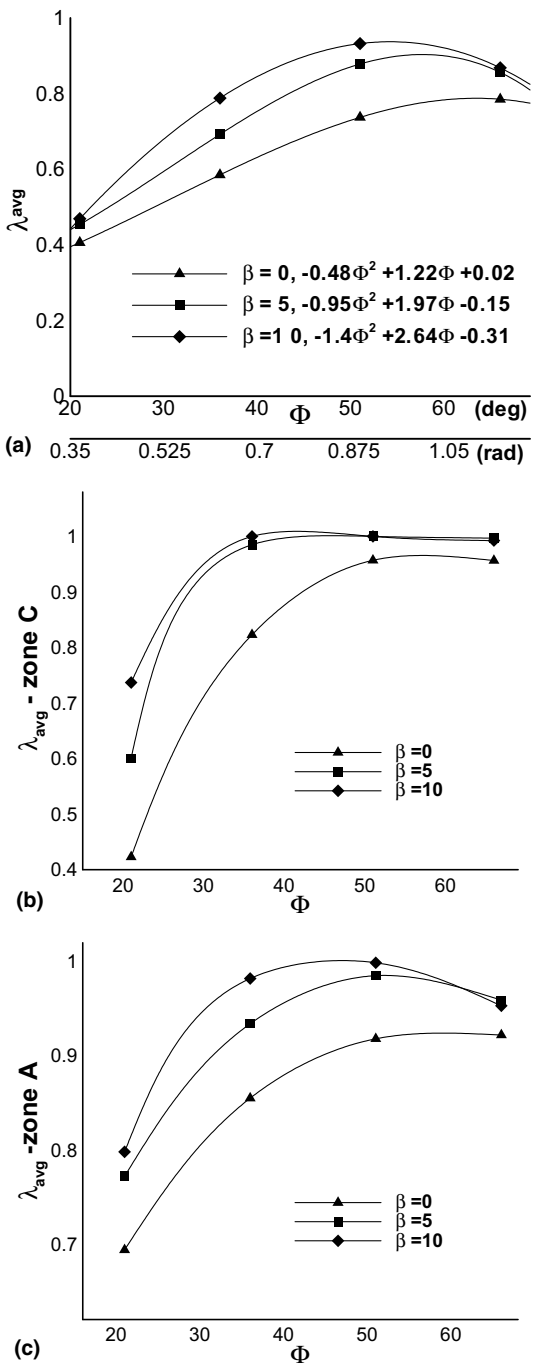

Fig. 8. Average liquid fraction (λ_{avg}) as a function of jet impingement angles (Φ and β) in degrees averaged over three different areas. (a) Entire windshield—the curve-fit is given for ϕ in radians, (b) Zone C, and (c) Zone A.

The area averaged non-dimensional heat transfer coefficient, $Nu_{avg} = (\int_{Area} Nu\, dA)/A$, is plotted in Fig. 13 as a function of time for the best and the worst configurations. Interestingly, the average peaks at about 900 s for both cases. This is due to fact that beyond this point the blower temperature becomes reasonably constant damping the growth of MID and OUT surface

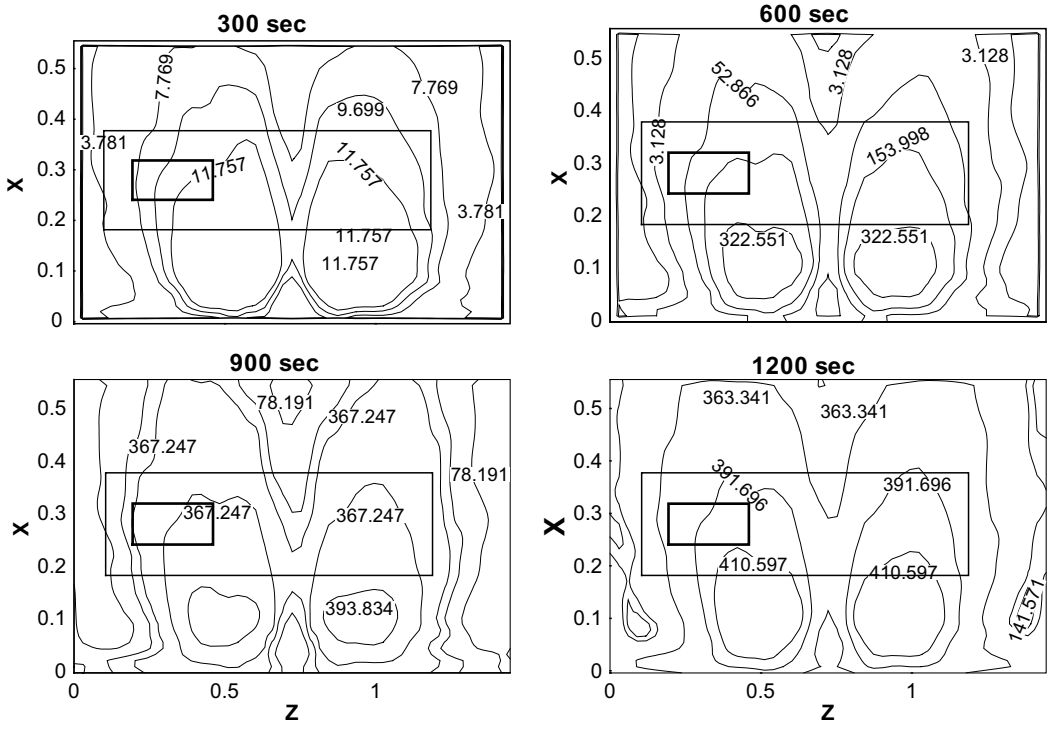

Fig. 9. Time evolution of the total enthalpy distribution for the best arrangement.

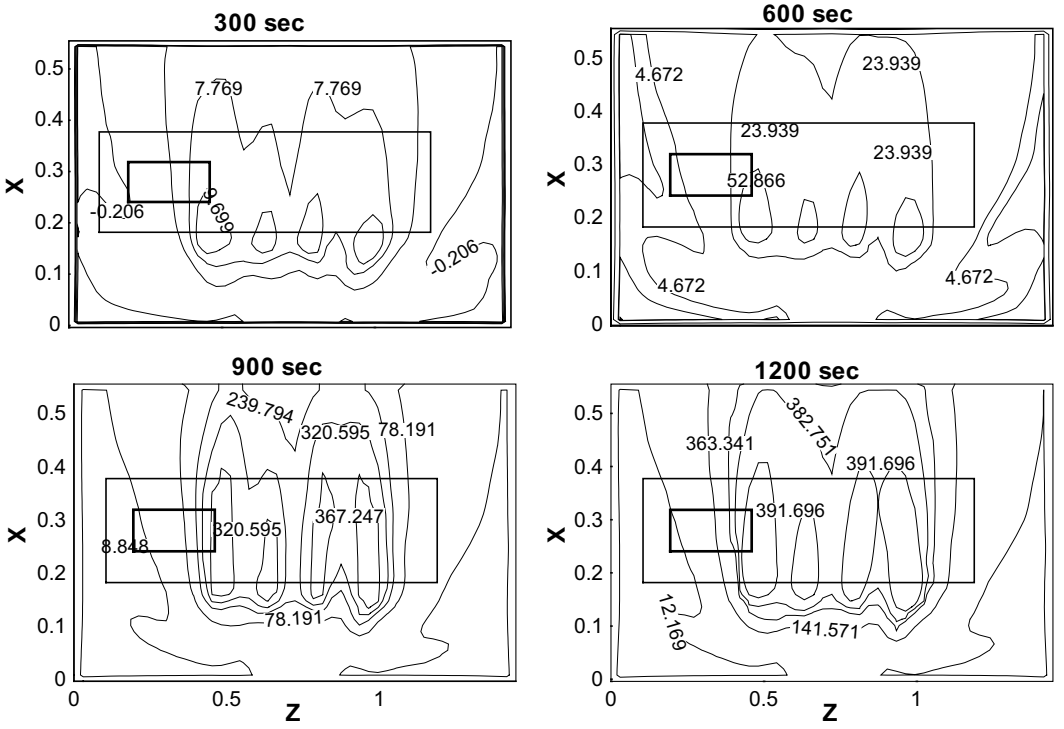

Fig. 10. Time evolution of the total enthalpy distribution for the worst arrangement.

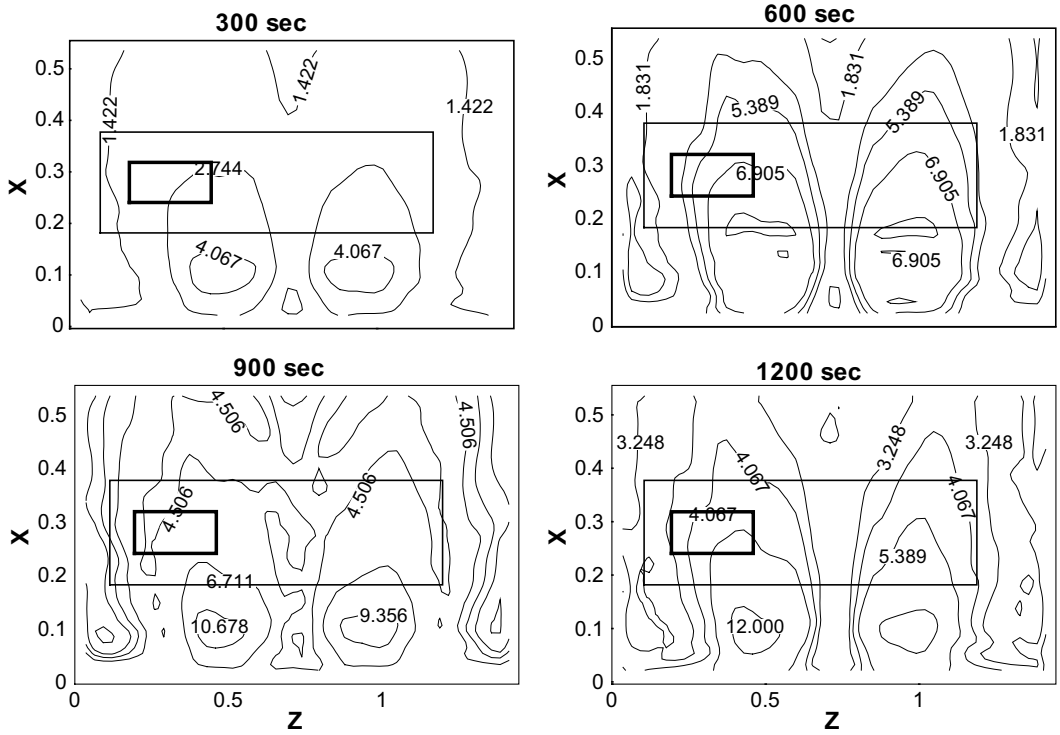

Fig. 11. Nusselt number distribution on the inner surface for the best arrangement plotted at four different time levels.

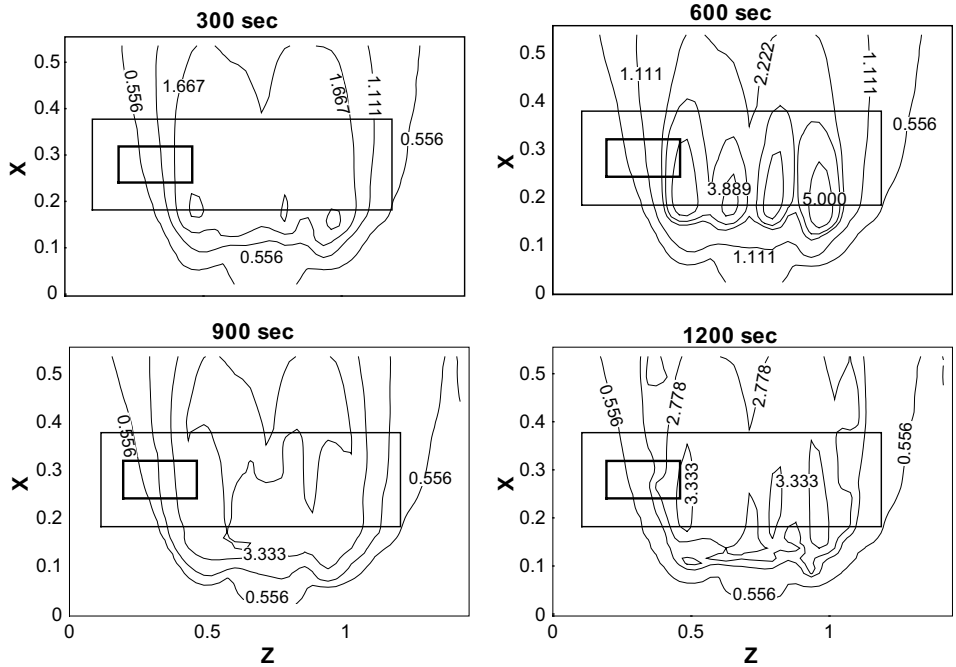

Fig. 12. Nusselt number distribution on the inner surface for the worst arrangement is plotted at four different time levels.

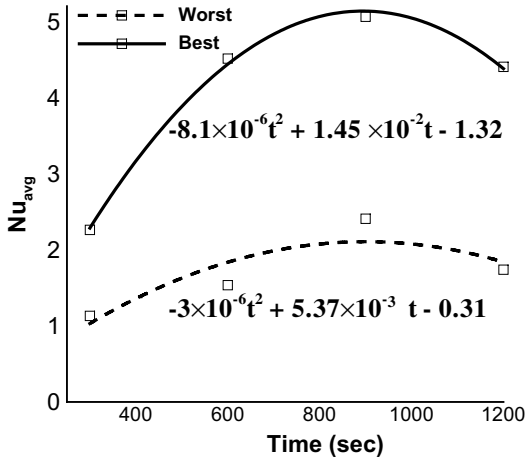

Fig. 13. Average Nusselt number calculated on the inner surface of the windshield as a function of time t seconds.

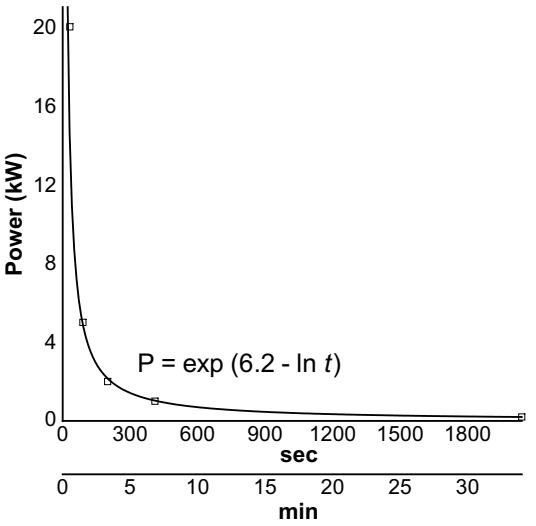

Fig. 14. Power required for the Joule heater to completely defrost the windshield within time t seconds.

temperatures. Thenceforth, the heat conducted due to the temperature gradient across glass thickness becomes dominant as compared to the heat convected outward. However, at their peak the best jet arrangement with $N_{\text{avg}} \approx 5$ is about 2.5 times more effective in transferring heat as compared to the worst arrangement with $Nu_{\text{avg}} \approx 2$. For 200 s $\leqslant t \leqslant$ 1200 s, the correlations for these two arrangements are found as follows:

(1) Best configuration, $\phi = 51°$ and $\beta = 10°$, $Nu_{\text{avg}} = -8.1 \times 10^{-6} t^2 + 1.45 \times 10^{-2} t - 1.32$
(2) Worst configuration, $\phi = 21°$ and $\beta = 0°$, $Nu_{\text{avg}} = -3 \times 10^{-6} t^2 + 5.37 \times 10^{-3} t - 0.31$

Power fit is again avoided for the aforementioned reason.

4.2. Case B

Fig. 14 plots the time required in case B to clear the windshield as a function of power applied to the ITO. The power requirement to defrost in 20 min is 369.5 W. As the power P increases the windshield clears faster. Eventually beyond 5 kW for which defrosting takes only 90 seconds, the power increases exponentially for a small reduction in defrosting time t. This has been correlated as, $P = \exp(6.2 - \ln t)$, where t is in seconds, and $P = \exp(2 - \ln t)$, for t in minutes. For power greater than 1.5 kW, further decrease in time spent defrosting the windshield may not be worth the extra power expended and the joule heater provides diminishing returns. However, for power levels of about 1.2 kW, the joule heater shows a clear superiority over the standard blower, requiring only 30% defrosting time of the traditional HVAC. While the power supply is not a part of this study, we note that this power level is acceptable assuming the engine is running, and the power can be supplied from the alternator. The reason for this superior performance of the Joule heater is the active heating mechanism that directly deposits heat to the ice layer through the glass, unlike the traditional blower heating system where air is utilized.

It is envisioned that in an improved version the ITO layer could be restricted only to the area mandated by safety standards (for example, region A in SAE J902 [15]), thus reducing the power requirements in efficient defrosting. The improved electrode design will also need less electrode material than the design modeled here.

5. Conclusions

The presence of two phases and the complex interaction of fluid thermal processes necessitate an efficient numerical simulation for its complete understanding and optimization. We present a deicing simulation for a practical three-dimensional geometry inside which hot air jets impinge upon a flat inclined glass surface with a layer of ice on the other side. Numerical analysis for varying flow and heat transfer characteristics inside this geometry was reported earlier. Here the unsteady process of melting of ice on the windshield is investigated using solidification and melting model. The main goal of the paper is to study the two-phase melting process over the inclined flat surface, and to identify the traditional control parameters such as jet impingement angles for minimization of the defrosting time for a given ice and glass thickness. Two correlations have been found for defrosting as functions of time, heat transfer parameters and impingement angles.

Also, in this study, the first joule heating defroster analysis using transparent electrodes are proposed and numerically simulated as a viable alternative. The predicted performance results are compared against the current jet impingement HVAC technology with respect to requirements in both time and power to melt the ice. A correlation between electrical power requirement in the proposed Joule heating defroster and the defrosting time is archived. It is demonstrated that substantial improvements in defrosting time (roughly 70% reduction in clearing time) may be made implementing the suggested design, which uses joule heating.

Acknowledgement

The authors were partially supported by the AFOSR, AFRL and NASA grants during the completion of this paper. The authors acknowledge many helpful discussions with Dr. Bashar Abdulnour, Dr. K.P. Singh, Mr. Paresh Patel and Mr. Sagar Kapadia.

References

[1] H. Martin, Heat and mass transfer between impinging gas jets and solid surfacesAdvances in Heat Transfer, 13, Academic Press, New York, 1977, pp. 1–60.
[2] S. Polat, B. Huang, A.S. Mujumdar, W.J.M. Douglas, Numerical flow and heat transfer under impinging jets: a review, Ann. Rev. Numer. Fluid Mech. Heat Transfer 2 (1989) 157–197.
[3] R.J. Goldstein, M.E. Franchett, Heat transfer from a flat surface to an oblique impinging jet, ASME J. Heat Transfer 110 (1988) 84–90.
[4] L. Huang, M.S. El-Genk, Heat transfer of an impinging jet on a flat surface, Int. J. Heat Mass Transfer 37 (1994) 1915–1923.
[5] S. Roy, K. Nasr, P. Patel, B. AbdoulNour, An experimental and numerical study of heat transfer off an inclined plane surface subject to an impingement airflow, Int. J. Heat Mass Transfer 45 (2002) 1615–1629.
[6] S. Roy, P. Patel, Study of heat transfer for a pair of rectangular jets impinging on an inclined surface, Int. J. Heat Mass Transfer 46 (2003) 411–425.
[7] D. Sahoo, M.A.R. Sharif, Mixed-convective cooling of an isothermal hot surface by confined slot jet impingement, Numer. Heat Transfer A 45 (2004) 887–909.
[8] I. Sezai, L.B.Y. Aldabbagh, Thee-dimensional numerical investigation of flow and heat transfer characteristics of inline jet arrays, Numer. Heat Transfer A 45 (2004) 271–288.
[9] H. Al-Sharqawi, N. Lior, Conjugate computation of transient flow and heat and mass transfer between humid air and desiccant plates and channels, Numer. Heat Transfer A 46 (2004) 525–548.
[10] M. Jeddi, S. Hannani, B. Farhanieh, Study of mixed-convection heat transfer from an impinging jet to a solid wall using a finite-element method—application to cook-top modeling, Numer. Heat Transfer B 46 (2004) 387–397.
[11] Stouffer and Sharkitt, Air sweep defroster, US Patent no. 464485, 1987.
[12] A. Aroussi, A. Hassan, Y.S. Morsi, Numerical simulation of the airflow over and heat transfer through a vehicle windshield defrosting and demisting, Heat Mass Transfer 39 (2003) 401–405.
[13] A. Farag, L.-J. Huang, CFD analysis and validation of automotive windshield de-icing simulation, SAE International, 2003-01-1079, 2003.
[14] R.W. Gent, N.P. Dart, J.T. Cansdale, Aircraft icing, Philos. Trans. R. Soc. Lond. A 358 (2000) 2873–2911.
[15] Surface vehicle recommended practice, Passenger Car Windshield Defrosting Systems, SAE J902, Review, July 2003.
[16] S.H. Lam, On the RNG theory of turbulence, Phys. Fluids A 4 (1992) 1007–1017.
[17] V.R. Voller, C.R. Swaminathan, A general source-based method for solidification phase change, Numer. Heat Transfer B 19 (1991) 175–189.
[18] V.R. Voller, C. Prakash, A fixed grid numerical modeling methodology for convection–diffusion mushy region phase-change problems, Int. J. Heat Mass Transfer 30 (1987) 1709–1719.